Spectral-elevation data registration using visible-SWIR spatial correspondence

Dalton Rosario[a] and Anthony Ortiz[b]

[a]U.S. Army Research Laboratory, 2800 Powder Mill Road, Adelphi, MD USA
dalton.s.rosario.civ@mail.mil
[b]University of Texas at El Paso, 500 W University Ave, El Paso, TX USA
amortizcepeda@miners.utep.edu

Abstract. We focus on the problem of spatial feature correspondence between images generated by sensors operating in different regions of the spectrum, in particular the Visible (Vis: 0.4-0.7 μm) and Shortwave Infrared (SWIR: 1.0-2.5 μm). Under the assumption that only one of the available datasets is geospatial ortho-rectified (e.g., Vis), this spatial correspondence can play a major role in enabling a machine to automatically register SWIR and Vis images, representing the same swath, as the first step toward achieving a full geospatial ortho-rectification of, in this case, the SWIR dataset. Assuming further that the Vis images are associated with a Lidar derived Digital Elevation Model (DEM), corresponding local spatial features between SWIR and Vis images can also lead to the association of all of the additional data available in these sets, to include SWIR hyperspectral and elevation data. Such a data association may also be interpreted as data fusion from these two sensing modalities: hyperspectral and Lidar. We show that, using the Scale Invariant Feature Transformation (SIFT) and Optimal Randomized RANdom Sample Consensus (RANSAC) algorithm, a software method can successfully find spatial correspondence between SWIR and Vis images for a complete pixel by pixel alignment. Our method is validated through an experiment using a large SWIR hyperspectral data cube, representing a portion of Los Angeles, California, and a DEM with associated Vis images covering a significantly wider area of Los Angeles.

Keywords: Shortwave IR, Visible, hyperspectral, Lidar, fusion, spatial correspondence.

1 INTRODUCTION

As flying drones continue to shrink in size and become lighter, and sensors also become more compact and lighter, the utility of these technologies become even more attractive to provide enhanced persistent local area coverage. Adding those facts with other motivating facts, such that hyperspectral sensors provide valuable information regarding the spectral characteristics of different materials of interest, while 3D point clouds provide a source of complementary information that can greatly assist in the classification of hyperspectral data, particularly when it is difficult to separate complex material classes [1-4], does close the loop in the scientific community's interest in exploiting these technologies for solutions aimed at improving situational awareness. Many techniques have been developed for fusion of hyperspectral and light detection and ranging (Lidar) data for classification purposes [5]. In 2013, the Data Fusion Technical Committee of the IEEE Geoscience and Remote Sensing Society (GRSS) organized a contest involving two data sets: a hyperspectral image and a Lidar derived Digital Elevation Model (DEM), both at the same spatial resolution (2.5 m), and two parallel competitions were established to devise advanced methods for fusion and classification of hyperspectral and LiDAR data. Many other examples can be found in classification of urban areas [1], but also in classification of complex forest areas [2]. As

challenging as the fusion contest have had been for its participants in 2013, a key facilitating fact about the GRSS dataset is that both types of data were simultaneously acquired, as the corresponding sensors were onboard the same flying platform. Both datasets were subsequently geo-rectified, requiring some manual intervention. This critical preprocessing step completely removed the requirement from participants to perform an often underestimated task: data registration; especially when datasets are of a different type.

Using Size, Weight, and Power (SWAP) constrained platforms, we focus on the problem of automatically fusing airborne hyperspectral data, collected from a small airplane, with the 3D Lidar-derived DEM of the same scene albeit collected by a different aerial platform and at a different date. Our emphasis is to achieve registration, or fusion, of these individual datasets, while not relying on corresponding metadata, especially on Global Positioning System (GPS) and Inertial Navigation System (INS) data. The problem addressed in this paper departs from the more traditional means of fusing geo-rectified hyperspectral data with geo-rectified 3D DEMs.

Our approach leverages multiple existing methods in the 3D reconstruction step of the overarching solution, to include Lowes's Scale Invariant Feature Transform (SIFT) [6] and incremental structure from motion via Snavely Bundler technique [7-8] to recover the 3D structure of the scene, using as input a set of overlapping images from the scene. And, motivated by the image-based localization method by Sattler et al. in [9] and the Optimal Randomized RANdom Sample Consensus (RANSAC) algorithm [10], we propose a method that registers 2D spatial information from hyperspectral data with the 3D Lidar-derived DEMs overlapping the same scene, yielding in the process the association between elevation data and material spectra in the Shortwave Infrared (SWIR: 1.0-2.5 μm) region of the spectrum. We accomplish this task by first addressing the problem of spatial feature correspondence between broadband SWIR and Visible (Vis: 0.4-0.7 μm). SWIR electromagnetic signals are appealing because of their robustness to visual impediments, such as fog, haze, and smoke.

To the best of our knowledge, results from our approach suggest for the first time to the scientific community that landmark scale-invariant spatial features in terrain SWIR images may indeed be used for pattern recognition in terrain Vis images. This correspondence is suggested by showing that our approach can successfully register terrain SWIR images to terrain Vis images representing the same scene. As a proof of principle, we use a large hyperspectral SWIR datacube representing a neighborhood of multiple city blocks of Los Angeles, California, USA; and a 3D Lidar-based DEM covering a significantly wider area of Los Angeles, but which includes the city's neighborhood featured in the SWIR data. Acquisition of both datasets was executed by two independent aerial platforms during time periods of many months apart. It is outside the scope of this paper, but the fusion between SWIR hyperspectral and elevation data can lead to the methodical use of spectral-elevation rules designed to segment the digitized scene into specific types of objects, such as, buildings, houses, tree clusters, grassy areas, and road/parking lots, which offers a significant value for Intelligence, Surveillance, and Reconnaissance (ISR) applications conducted in both civilian and military communities. As an example, we focus on the Intelligence Preparation of Battlespace (IPB) [11].

IPB is recognized as an essential element of the intelligence cycle. This is evidenced by its inclusion as one of the six intelligence and electronic (IEW) tasks described in the US Army's intelligence principles manual. The categories of IEW products are IPB, situation development, indications of warnings, target development and acquisition, and force protection. Battlespace is the environment, factors, and conditions that must be understood to successfully apply combat power, protect force, or complete the mission. IPB is an analytical methodology employed to reduce uncertainties concerning the enemy, environment, and terrain for all types of operations. IPB builds an extensive database for each potential area in which a unit may be required to operate. The database is then analyzed in detail to determine

the impact of the enemy, environment, and terrain on operations and presents it graphic form. IPB is a continuing process.

The remainder of this paper is organized as follows: Section 2 discusses the relevance of hyperspectral imagery contributions to IPB products, Section 3 discusses the datasets used in this research, Section 4 proposes the 3D model-hyperspectral data fusion, Section 5 discusses the results, and Section 6 draws some conclusions.

2 RELEVANCE OF PROBLEM

A successful method for automatic image registration, using images generated by independent SWIR and Vis cameras, may enable the automatic data fusion from different sensing modalities (e.g., SWIR and Lidar DEM), especially taking into account that elevation data collections often include Vis cameras as an attempt to associate visible with elevation measurements. If hyperspectral or multispectral remote sensing is one of the sensing modalities, such a data fusion enables further the automatic segmentation of key materials from the subject digitized terrain, yielding in the process high value 3-dim material segmented maps for ISR analysis. With SWIR signal robustness to environmental scene degradation and ISR decision makers in mind, IPB in particular helps the commander selectively apply and maximize his/her combat power at critical points in time and space, it is also designed to support staff planning the commander's loop in observing, orienting, deciding, and acting. Therefore, IPB is a continuous, systematic process of analyzing weather, enemy, and terrain information in a specific geographic area [11]. Key IPB products includes: (i) Modified Combined Obstacles Overlay, (ii) Doctrinal Template, (iii) Situational Templates, (iv) Event Templates, (v) Course of Action Sketches, and (vi) Decision Support Templates. Conceptually, IPB analysts use an N-dim map terrain consisting of many components that are stacked and spatially aligned over each other, to include: Social Network 2-dim map, Belief System 2-dim map, Language 2-dim map, Infrastructure 2-dim map, Cyber 2-dim map, Information 2-dim map, and Geospatial 2-dim map. Among the various components the Geospatial is the one that most apply for this paper. The Geospatial dimension may be interpreted as a material segmented 2-dim map of the terrain, where it is valuable to show in the map reliable information about the spatial locations and distributions of clusters of trees (threats, for instance, may be hidden beneath heavy tree clusters), line of communications (roads and rivers, for potential evacuation or approach), grassy areas, body of water (for mobility/trafficability analysis), manmade structures (high buildings, house neighborhoods).

This section identifies and discusses a number of the ways hyperspectral data contribute to IPB and related activities. While not written as an exhaustive list, in what follows IPB elements are given as bullets followed by one or more spectral applications (in italic). Applications are divided according to whether they provide a principal or supplementary contribution to the problem. Examples of these applications are found below.

- Principal contributions:
  - Interesting aspect of terrain
    - Cover and concealment
      Landcover classification
      Hide area delineation
    - Obstacles
      Mobility trafficability analysis
  - Identification of the threat
    - Threat detection
      Detection of target in open
      Detection of sub-pixel target
    - Counter Camouflage Concealment & Deception

> > > *Detection of camouflage nets*
> > > *Detection of concealed targets*
> > ▪ Lines of communication
> > > *Determination of road and other transportation networks*
> > ▪ Threat activity
> > > *Determination of stressed vegetation*
> > > *Vegetation burn index*
- Supplementary contributions:
  - Aspect of terrain
    - ▪ Observation & fields of fire
      - *Battlespace perspective viewing Viewshed*
      - *(threat dome) analysis*
    - ▪ Key terrain
      - *Detection of landing strips*
  - Aspect of weather
    - *Characteristics of atmosphere for visibility*
    - *Cloud cover*
    - *Temperature from longwave IR*
  - Other characteristics of the battlespace
    - *Detection of buildings and other logistics infrastructure.*

3 DATASET

SWIR hyperspectral and elevation data are of particular interest to this work. We used an existent dataset collected by Headwall Photonics over a multi-block urban area of downtown Los Angeles, California, USA, using Headwall's Hyperspec® SWIR hyperspectral imaging sensor [12] onboard a small manned airplane. Key sensor specifications: 384 spatial bands, 260 spectral bands, wavelength range 0.9-2.5 μm, maximum frame rate 450 Hz, Stirling-cooled MCT detectors, weight of 4.4 kg, aberration corrected imaging, all-reflective concentric optical design, collect full spectrum range for every pixel in field of view. The manned airplane flew the *pushbroom* hyperspectral imaging system over the target area in Los Angeles, collecting 829 samples by 260 SWIR bands (defined in this case as a frame) and using the airplane's movement to obtain 1,163 lines. A representation of the datacube consisting of 1,163 lines by 829 samples by 260 bands of the target area in Lost Angeles is shown as the band average (less than 1 m pixel resolution) in Fig. 1 (top), next to its correspondent *Google Map* color image Fig. 1 (bottom).

The area represented in Fig. 1 includes live vegetation (trees, grass) and manmade structures (high buildings, houses, roads, and parking lots, and other unknown manmade objects). Data acquisition to obtain these images occurred 24 months apart, where the SWIR data acquisition happened closer to sunset; explaining the prolonged shadows observed near the high buildings. We hypothesized that scale invariant features of terrain landmarks between SWIR images and their correspondent Vis color images correspond to each other; thus, we decided to explicitly explore this intuition as part of our image registration approach.

Regarding the elevation measurements, we used a 3D DEM of a significantly larger area of Southern California, containing a large portion of the Los Angeles County, to include mountains and the entire downtown Los Angeles. The DEM is geo-rectified for Latitude and Longitude world coordinates per pixel of equal size (1 m spatial resolution), and includes both elevation measurements from a Lidar system and geo-rectified wide area orthophoto (nadir Visible color image) to put scene context in the DEM, see Fig. 2.
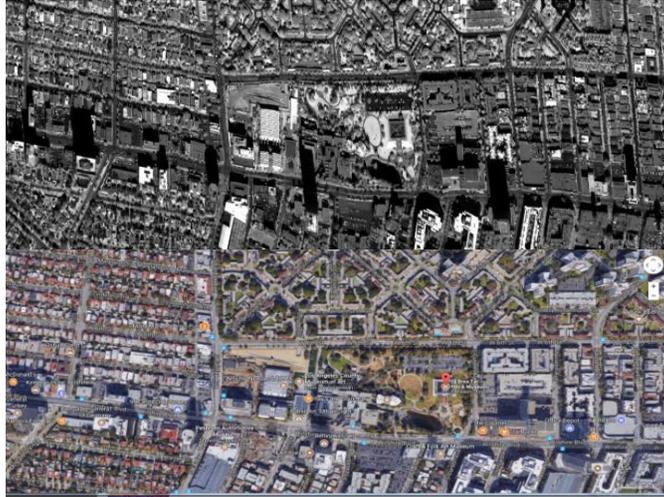
Fig. 1. SWIR hyperspectral band average (top) of a multi-block urban region of Los Angeles, USA, next to its correspondent Google Map image (bottom). The area includes live vegetation (tree, grass) and manmade structures (e.g., roads, parking lots, high buildings, houses). By visual inspection one can notice the spatial feature similarities between the SWIR and Visible color images, which we plan on automatically extracting and exploring for image registration.

Fig. 2. 3D Digital Elevation Model (1 m pixel resolution) of a portion of Los Angeles County, California, USA, which includes in relative scale the multi-block downtown portion of Los Angeles where the SWIR hyperspectral data were collected. The image registration method that found the correct spatial location is discussed in Section 5.

Fig. 2 depicts the DEM and shows in relative scale the spatial area where within the DEM spatial area the SWIR data acquisition occurred; but of course this spatial location was unknown prior to the execution of our image registration method using these two independent regions of the electromagnetic spectrum: SWIR and Visible. The orthophoto provided with the DEM covers an area that are many orders of magnitude larger than the area covered by the SWIR datacube. In the scope of this paper, the successful registration by a machine using

these image sets constitutes a successful automatic association of elevation data with spectra, given that for each aligned pixel between these two images there is a corresponding spectrum available in the hyperspectral datacube. Our image registration approach is discussed next.

4 FUSION APPROACH FOR 3-D DEM AND HYPERSPECTRAL DATA

Inspired by image-based localization approaches similar to the one introduced by Sattler et al. in [9], and the Optimal Randomized RANSAC algorithm [10], we propose the approach depicted in Fig. 3 to register the 2D spatial area of hyperspectral data cubes onto an available 3D DEM that includes the hyperspectral target scene in order to associate elevation measurements with each spectra, as follows:

(a) The fusion starts by representing each 3D point by all the SIFT descriptors contributing to its value from the reconstruction. All the descriptors of a single 3D point are assigned to a visual word. If more than one descriptor is coming from the same image, the mean of those SIFT descriptors is used to represent the contribution of that image to the 3D point. The K-means clustering algorithm is applied to cluster all the 3D point clouds into k clusters. We used 100,000 clusters in this experiment, given the size of the 3D reconstruction.

(b) To improve computational efficiency, while facilitating convergence into a solution, we avoid comparing all of the points in the point clouds by assigning the centroids obtained from the k-means to be the visual words, as shown in Fig. 3.

(c) SIFT is independently computed on the SWIR and Visible reference images and results are represented as visual words for comparison with visual words from (b) (see Fig. 3, and details in *Table I*.)

(d) The visual word comparison strategy can then be reduced by finding through a sequential search the two nearest visual words in (b) to the visual word (hyperspectral-based SIFT descriptor) in (c).

(e) The sequential search in (d) yields as set of correspondences between each hyperspectral-based SIFT descriptor and two 3D model visual words. A correspondence is accepted if the two nearest neighbors pass the SIFT ratio test with a certain threshold. This is based on the idea that the probability that a match is correct can be determined by taking the ratio of distance from the closest neighbor to the distance of the second closest [6]. The method rejects all matches in which the distance ratio is greater than 0.7. This threshold works empirically well for this dataset. If more than one 2D-feature matches exist in association with the same 3D point, the descriptor with smallest Euclidean distance is selected.

(f) The linear search continues until a user-specified number of correspondences (Nt) is satisfied (in this experiment this number was set to 100), or the search is exhausted from the hyperspectral data perspective.

(g) The correspondence set obtained in (f) does not necessarily guarantee a geometric alignment of the hyperspectral images onto the 3D DEM that would match the quality that could be achieved with human intervention. In order to improve the alignment process, we applied the Optimal Randomized RANSAC algorithm to the set of correspondence vectors obtained in (f). The geometric alignment is declared as acceptable using the criterion that more than n correspondences ($n = 5$ works well empirically in this dataset) must be inliers to accept a match. See *Table I* for more details.

The fusion algorithm summarized in Table 1 also applies to the specific case when a 3D reconstructed model from photogrammetry is available with the correspondent photos in which the structure from motion approach can be employed. We re-emphasize to the reader that fusion in this context, beyond the obvious registration between 2D photos and band

images, means being able to associate 3D elevation with spectral data after the 2D image registration process is accomplished.

TABLE 1
ALGORITHM: HYPERSPECTRAL-3D MODEL DATA FUSION

```
REQUIRE:       (HSI, 3D_PointClouds, distRatio,
max_nbMatches, inlier_ratio, nb_Inliers,
ransacTime)
ENSURE: HSI_3D_Mapping

clusterFile ← k-means(3D_PointClouds)
kdtree ← flann->generate_kdtree(clusterFile)
HSI_vw ← getSIFT(HSI)
nb_matches ← 0
for each (i ∈ {HSI_vw}) do
    if (nb_matches < max_nbMatches) then
        {vw1,vw2} ← vw_s from kdtree closest to i
        if       ((L2Dist(vw1,i)/L2Dist(vw2,i)) <
distRatio) then
            nb_matches ++
            matches ← (i, vw1)
        end if
    else
        break for loop
    end if
end for
while (time in this loop < ransacTime) do
    1.Select four feature pairs randomly from
correspondences.
    2.Compute homography H (exact).
    3.Compute ransac_inliers where:
    SSD(p'_i, Hp_i) < inlierRatio
    4.Keep largest set of inliers and
corresponding homography H.
    5.Re-compute least-squares H estimate on
all of the inliers.
end while
if ransac_Inliers >= nb_Inliers then
    Build 3D-HSI using H and matches
else
    Print HSI not found in 3D-model
end if
return 3D-HSI                    ▷ Fusion is complete
```

The approach depicted in Fig. 3 also applies to the fusion of the available SWIR hyperspectral datacube with geo-rectified 3D DEM (obtained from Lidar measurements); albeit with a key difference. As the DEM of the Los Angeles County also included the correspondent overlaid orthophotos, the matching search only considers the SIFT descriptors from the downtown SWIR image and the wider area DEM orthophoto. As discussed in Section 5, results from our experiment using our approach validate our intuition that these landmark descriptors are highly correlated between SWIR and Visible images of the same scene.
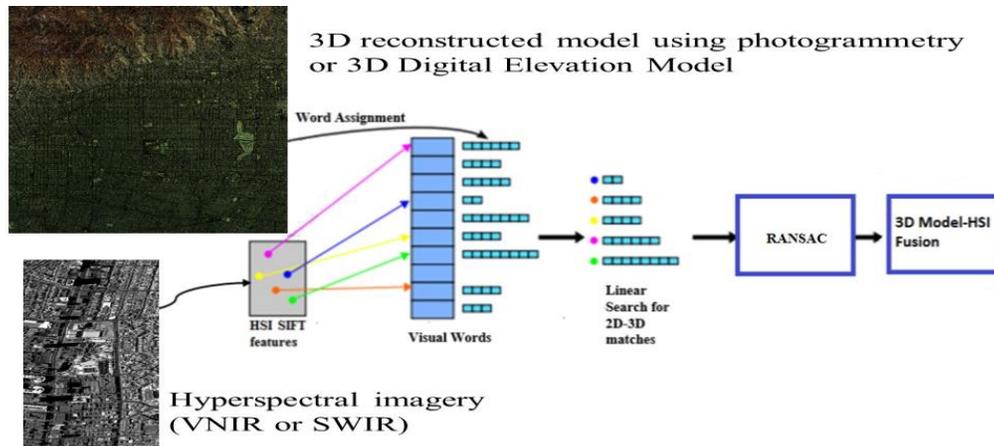
Fig. 3. 3D model-hyperspectral data fusion.

5 RESULTS AND DISCUSSION

The fusion approach described in Section 4 was applied to the hyperspectral SWIR dataset and Visible orthophotos of corresponding DEM using the following details.

We chose band 14 (near 1.2 μm) to represent the spatial area of the entire SWIR hyperspectral datacube because of the high reflectance property of most material types in an urban scene, relative to other bands. In order to address more efficiently the computational load and associated time, given the vast spatial coverage of the DEM relative to the hyperspectral SWIR spatial coverage (see Fig. 2), we split in half the spatial area of SWIR band-14 and allowed each half to compute their spatial matches independently of each other, such that each half estimated its spatial feature matches within a neighborhood centered at a random (without replacement) spatial location in the wide-area Visible orthophoto, thus eliminating once for all the undesirable locations in the wide-area digitized scene and retaining the better prospects. This proposed approach is highly effective because it allows the computational load, which is O^2 relative to the spatial area, to be processed in parallel using two smaller areas rather than simultaneously using a single twice-as-large spatial mosaic, cutting in half the matching-search computational time. This reduction rate is also independent of the employed CPU (central processing unit) or GPU (graphics processing unit). So, the benefit for using this approach is twofold: (i) the split-and-conquer strategy allows for an O^2 computational time reduction that is linearly proportional to the number of splits (e.g., 2, 3, 4), as it allows for parallel processing, and (ii) the random-without-replacement-location-withdraw strategy allows for the execution of a significantly more efficient search relative to systematically processing every location across the spatial area of the wide-area Visible orthophoto.

Our matching search strategy paid off by yielding the local match result depicted in Fig. 4, where the gray area represents the SWIR spatial area overlaid onto the larger local neighborhood in the Visible orthophoto that produced the best matching result. Notice in Fig. 4 that the split match is slightly misaligned, since they were performed independently from each other. We could rectify this misalignment by applying our matching search approach as a last step between the entire SWIR mosaic and the neighborhood where this split conversion occurred in the Vis orthophoto; this optimization, however, was not done for this paper. The real advantage from this spatial match is that each voxel in the SWIR datacube not only features 270 bands but also has a corresponding elevation from the DEM.

Fig. 4. Successful registration between the SWIR band image (embedded gray scale image in the center) and a spatial location within the DEM's orthophoto (larger image).

Using this data association, one can generate IPB products based on spectral and elevation properties as discussed earlier. For instance one could apply material property indexes (e.g., wetness index) to the fused data in order to segment the scene into main material types, such as materials in the scene containing large concentration of water (e.g., live vegetation (trees, bushes, and grass)) and dry materials (e.g., manmade structures (roads, buildings, houses)). Using the elevation data in conjunction with the material wetness segmented map, for instance, a method can be developed to provide further segmentation in the scene, to include the spatial locations of high buildings, low houses, high trees, low grass areas, parking lots/roads, etc. Demonstrating this capability, however, is beyond the scope of this paper.

6 CONCLUSION

We proposed a fusion method that uses as input aerial nadir-view hyperspectral imagery and corresponding photos associated with DEMs created from Lidar data; and showed, using SIFT and Optimal RANSAC algorithm, that spatial correspondence exist and can be successfully employed for spatial registration between SWIR and Vis images. To the best of our knowledge, this spatial correspondence has never been reported in the literature as a means to register imagery generated by these two sensing modalities. Results from this work can be used with other higher level methods (e.g., spectral-elevation rule based approaches) to produce terrain segmented maps of high value for IPB and other surveillance and reconnaissance applications. The advantages of our approach are summarized as follows.

Robustness in GPS denied or degraded environment: Because the data registration between both modalities (hyperspectral and elevation data) is performed based on spatial features and does not rely on using GPS or INS (inertial navigation system (INS)) measurements to bring both data sets into the world coordinates, the approach may be applied using data from different aerial platforms under GPS denied or degraded environment. For instance, this approach could be applied to a scenario where hyperspectral data acquisition was conducted using an aerial platform, to include a small drone, at the point of need and under a GPS denied or degraded environment, while elevation data (e.g., Lidar data) of the target area collected by an independent aerial platform are available and geo-rectified. In this scenario, the approach may be interpreted as a method that can geo-rectify the hyperspectral data cube(s), while associating spectra with elevation data for additional processing that can further segment the digitized terrain—using for instance spectral-elevation rule based properties—into key material types (live vegetation (specifically separating high tree clusters from low grassy areas), water, and manmade structures (specifically separating high buildings from lower elevation houses).

Robustness to visually degraded conditions: In principle, one can leverage the natural SWIR electromagnetic waves' robustness to visual atmospheric obscurations to produce material segmented maps from data collected during degraded conditions (fog, haze, or smoke), given that we showed that key scale-invariant spatial features in SWIR images can be used for pattern recognition in corresponding spatial features in Vis images.

Flexibility in 3D visualization: The ability to successfully register data that are not geo-rectified with data that are geo-rectified opens additional windows of opportunity, to include further processing to produce terrain segmented maps ready to be visualized using standard 3D viewers that operate in the world coordinates, e.g., Google Earth.

References

[1] Lemp, D. and Weidner, U., "Segment-based characterization of roof surfaces using hyperspectral and laser scanning data," *Proc. IEEE Int. Geosci. Remote Sens. Symp.* **7**, 4942–4945 (2005) [https://doi.org/10.1109/IGARSS.2005.1526783].

[2] Dalponte, M., Bruzzone, L., and Gianelle, D., "Fusion of hyperspectral and LIDAR remote sensing data for classification of complex forest areas," *IEEE Trans. Geosci. Remote Sens.* **46**(5), 1416–1427 (2008) [https://doi.org/10.1109/TGRS.2008.916480].

[3] Weng, Q., "Remote sensing of impervious surfaces in the urban areas: Requirements, methods, and trends," *Remote Sensing of Environment* **117**, 34-49 (2012) [https://doi.org/10.1016/j.rse.2011.02.030].

[4] Ghamisi, P., Couceiro, M.S., Martins, F.M., and Benediktsson, J.A., "Multilevel image segmentation approach for remote sensing images based on fractional-order Darwinian particle swarm optimization," *IEEE Trans. Geosci. Remote Sens.* **52**(5), 82-102 (2014) [https://doi.org/10.1109/TGRS.2013.2260552].

[5] Wang, H., Glennie, C., and Prasad, S., "Voxelization of full waveform LiDAR data for fusion with hyperspectral imagery," *Proc. IEEE Int. Geosci. Remote Sens. Symp.*, 3407–3410 (2013) [https://doi.org/10.1109/IGARSS.2013.6723560].

[6] Lowe, D.G., "Distinctive image features from scale invariant key points," *International Journal of Computer Vision* **60**, 91–110 (2004) [https://doi.org/10.1023/B:VISI.0000029664.99615.94].

[7] Snavely, N., Seitz, S.M., and Szeliski, R., "Photo tourism: exploring photo collections in 3D," *ACM Trans. on Graphics (TOG)*. **25**, 835–846 (2006) [https://doi.org/10.1145/1179352.1141964].

[8] Snavely, N., Seitz, S.M. and Szeliski, R., "Modeling the world from internet photo collections," *International Journal of Computer Vision* **80**, 189–210 (2008) [https://doi.org/10.1007/s11263-007-0107-3].

[9] Sattler, T., Leibe, B., and Kobbelt, L., "Fast image-based localization using direct 2d-to-3d matching," *Proc. IEEE International Conference on Computer Vision*, 667–674 (2011) https://doi.org/10.1109/ICCV.2011.6126302].

[10] Chum, O., Matas, J., "Optimal randomized RANSAC," *IEEE Tran. Pattern Analysis and Machine Intelligence* **30**, 1-11 (2008) [https://doi.org/10.1109/TPAMI.2007.70787].

[11] Army, U.S., "Doctrine & Training," *Army Publishing Directorate*, (2018) [https://armypubs.us.army.mil].

[12] Grim, K, "Headwall photonics product specs," *Headwall Photonics website* (2018) [http://www.headwallphotonics.com/].